The influence of a dielectric spacer layer on the morphological, optical and electrical properties of self-dewetted silver nanoparticles

Leila Manai, Béchir Dridi Rezgui, Damien Barakel, Philippe Torchio, Olivier Palais, Olfa Messaoudi, Arwa Azhary, Feriel Bouhjar, Brahim Bessais

The influence of a dielectric spacer layer on the morphological, optical and electrical properties of self-dewetted silver nanoparticles

Leila Manai[a,b], Béchir Dridi Rezgui[b], Damien Barakel [c], Philippe Torchio[c], Olivier Palais[c], Olfa Messaoudi [a], Arwa Azhary[a], Feriel Bouhjar[d] and Brahim Bessais[b]

[a]Physics Department, College of Sciences, University of Ha'il, Ha'il, Saudi Arabia; [b]Research and Technology Center of Energy, Photovoltaic Laboratory, Borj Cedria Science and Technology Park, University of Tunis El Manar, Campus Universitaire de Tunis El Manar, Tunis, Tunisia; [c]Institut Matériaux Microélectronique Nanosciences de Provence-IM2NP, Aix Marseille Université, CNRS-UMR 7334, Domaine Universitaire de Saint Jérôme, Service 231, Marseille, France; [d]Department of Physics, College of Science and Humanities, Al Quwayiyah, Shaqraa University, Al Quwayiyah, Saudi Arabia

ABSTRACT

Metal nanoparticles attract the worldwide interest due to their interesting optical and electrical properties, which allow their implementation as promising light scatters in solar cell devices. These nanoparticles exhibit localized surface plasmon resonance (LSPR) characteristics, which are strongly dependent on both intrinsic and extrinsic factors. Tuning the LSPR characteristics yields to interesting properties in terms of enhancement, localization and guiding of the electromagnetic field on sub-wavelength scales. For that purpose, we investigate in this work the effect of dielectric spacer layer (tin oxide) with different thickness on light reflection due to random self-assembled Ag-NPs. A correlation between morphological properties, optical reflectance and electrical characteristics is established by combining scanning electron microscopy, UV-Vis-NIR spectroscopy and current–voltage analyses. Our results show that a dielectric layer with an appropriate thickness and refractive index is useful for reducing the amount of reflected light and consequently the shifted photocurrent response for all wavelengths.

Introduction

Energy is an essential requirement for life nowadays, since it is indispensable for continued human development and economic growth. The global energy market is dominated by fossil fuels such as oil, coal and natural gas. These sources are unsustainable, exhaustible, cost-ineffective and environ- mentally damaging. In fact, the combustion of fossil fuels will release a great deal of carbon dioxide (CO_2), which exacerbate global warming. Besides, the excessive use of such sources caused by the high demand on energy will deplete them in few decades. Renewable alternative energy resources are free, inexhaustible and widely available across the planet at low cost. Moreover, they have the potential to meet the future energy demands with a minimal environmental impact [1]. Within the range of renewable energies, Photovoltaic energy has already showed its achievement and wide- spread applications for solar energy utilization. Photovoltaic technology provides an ecofriendly and sustainable energy route to convert light energy, composed of photons, directly into electricity without any intermediate stage. To effectively achieve this potential, it is crucial to realize high-

conversion efficiency for the solar cells. Nowadays, scientists devote their efforts to design solar devices with high-conversion efficiency, large-scale implementation and low cost [2–4] but still did not accomplish their effective goals. Nevertheless, the important development of photovoltaic market on a global scale need an efficient improvement regarding materials to reduce their fabrica- tion high cost and increases their conversion efficiency. One of the key factors that can boost the performance of solar cells is the enhancement of light trapping into the photo-absorbing layer [5,6]. In recent years, nanoplasmonics has emerged as one of the best solution to achieve this goal [7–12]. Noble metal nanostructures, supported by surface plasmons resonance mechanism, showed the ability to concentrate and guide light at the nanoscale. In fact, surface plasmons (SPs) are considered as the collective oscillations of conduction electrons between the interface of metal nanoparticles (M-NPs) and a dielectric. Due to their evanescent nature, SPs are capable of giving rise to particular interaction with light. When excited under an electromagnetic wave sufficiently near the resonance frequency, an intense absorption and/or scattering of light is gener- ated [13]. The increase of absorption is called also the near-field enhancement, because it consists of the capacity to locally focus light around the surface of M-NPs by generating a near-field enhance- ment [14]. Hence, in this situation, M-NPs can be described as nano-scale concentrators enabling the collection of photons from an area much larger comparing to the physical particle size. The rest of field can propagate further at high angles, inducing light trapping via scattering. This mechanism presents the second mechanism of localized surface plasmon resonance (LSPR), which is the far- field enhancement. In fact, M-NPs can scatter light and thus enable redirecting the initially incident light for privileged scattering into the active area of solar cell [15]. Light can be coupled into the active layer of the solar cell, inducing an enhancement in the photo-electric current. The resonant behavior of the M-NPs makes them a flexible and an efficient tool to be integrated in solar cell devices and can be used to manipulate and enhance light trapping, and thus to probably increase the conversion efficiency. The LSPR frequency, intensity and width of the M-NPs can be tuned by changing their size, type, shape, distribution, dielectric spacer between them and the semi-conduc- tor or their surrounding medium [16]. This leads to the modification of the spectral profile of the absorbed power in the active area of the cell providing an improvement in the photo-electric cur- rent. In particular, the effect of the underlying dielectric environment on LSPR attracted a great deal of interest. Several reports showed that the resonance characteristics of M-NPs depend on the sur- rounding medium. Beck et al. [17] have recently showed that the surface plasmon resonance wave- length is red-shifted by increasing the under-layer refractive index, from 500 nm for self-assembled particles on SiO_2 to 700 nm for particles on TiO_2. Through this variation of the local dielectric environment of plasmonic nanoparticles, the optical absorption in an underlying silicon wafer is increased five-fold at 1100 nm and the external quantum efficiency of thin silicon-based solar cells is enhanced by a factor of 2.3 at this wavelength. In addition to the refractive index, the dielec- tric layer thickness is as well an essential factor that determines the surface plasmon effect. Nano- particles on an oxide spacer have high driving field intensities, forming a larger normalized scattering cross section in the long wavelength region [18,19]. In this work, we investigate the effect of dielectric spacer layer (SnO_2) with different thickness on light reflection due to random self-assembled silver nanoparticles (Ag-NPs), indicating that a dielectric layer with an appropriate thickness and refractive index is useful for reducing the amount of reflected light and consequently the shifted photocurrent response for all wavelengths. These different behaviors are determined by whether the dielectric layer is beyond the domain where the electric field of silver plasmons takes effect, combined with the effect of geometrical optics. By measuring the optical and electrical prop- erties of the solar cell device, the plasmonic behavior is determined when placed on full-scale device.

Experimental

The process of cell fabrication of the self-assembled Ag-NPs/c-Si structure is carried out through several consecutive steps. Mono-crystalline silicon produced by Czochralski, doped boron (B)

with the orientation (100) is used in this work. Prior to doping, silicon wafers were initially ultra-sonicated sequentially at 40°C in acetone, isopropanol and deionized water for 10 min in order to remove organic and inorganic impurities. The cleaning continues with an etching step for 3 min in diluted (5%) hydrofluoric acid solution that results in flat silicon wafer surface. For achieving a p-n junction, p-type silicon wafer is undergo to the new dopant phosphorus (P) atoms which can be diffused into the material through concentration gradient. The process is performed by thermal physical vapor deposition system at

high temperature. Liquid phosphoryl chloride (POCl$_3$) is trans- ported to silicon wafers via nitrogen carrier gas in the furnace at 930°C. Oxygen flow (O$_2$) is used to help the creation of n-type layer according to the equations:

4POCl$_3$ + 3O$_2$ 2P$_2$O$_5$ + 6Cl$_2$ (1) P$_2$O$_5$ + Si SiO$_2$(P) (2)
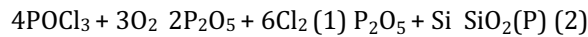
According to these two equations, the silicon surface phosphorus silicate glass is formed. During the doping process, the formed n-layer takes place all over the surface including the front, back and edge sides of the wafer. In this situation, there is a need to an edge and back isolation in order to prevent short circuit and recombination of electron–hole which disable the cell operation. Metal contacts are created then in front and back side of the p-n junction in order to allow the absorption of light and to better collect the separated charges. In the back side, we deposited 500 nm of alumi- num by thermal evaporation, while for the front side; silver of 300 nm is required. Then, samples are annealed in rapid thermal processing furnace at 550°C during 15 min to ensure the metal diffu- sion. Tin oxide (SnO$_2$) with different thicknesses were evaporated by a thermal evaporator at low deposition rate (0.1 Å/s). Samples with dielectric layer thicknesses ranging from 20 to 152 nm pro- vided a dielectric environment for plasmonic nanoparticles. After the deposition of SnO$_2$, a 15 nm of silver film were evaporated on all substrates followed by a thermal annealing at 250°C during 1 h. Figure 1 shows a schematic 3D representation of the investigated structure.

Total reflectance as a function of wavelength R(λ) characterizations was performed using a Per- kin Elmer (Lambda 950 UV-Vis-NIR) spectrophotometer equipped with an integrating sphere in the wavelength range of 250–2500 nm (with 2 nm step). Samples were characterized by spectro- scopic ellipsometry (GES5E Spectroscopic Ellipsometer) in order to determine the refractive index n and the extinction coefficient k of SnO$_2$ and Ag. Thicknesses of SnO$_2$ and Ag are deter- mined using two techniques: ellipsometry and profilometry. We obtained accordance between values determined directly by the profilometer and those determined after ellipsometry analysis (with a precision of 1 nm). The morphology of Ag-NPs was qualitatively and quantitatively ana- lyzed using a Field Emission Scanning Electron Microscopy (FESEM, Zeiss ULTRA 55 model equipped with an In-Lens SE detector) and image processing and analysis software (Image J) [20].

Figure 1 . Schematic representation of the experimental design.

To electrically characterize samples, we used a solar simulator under standard conditions: (air mass 1.5 Global filter (AM1.5G), with intensity of 1000 W/m^2) equipped with an integrated shutter. The external voltage was supplied by an Agilent 3640A programmable DC power supplies and the current was measured using a Keithly 2000. Another physical measurement that can be used to evaluate the performance of the solar cell is the spectral response SR(λ). We used an ASB-XE- 175 Xenon Fiber Optic Source to generate illumination spectrum from UV to NIR (200 to 1180 nm). A monochromatic spectrum was obtained from DK240 1/4 meter monochromator (offered by Spectral Products) modulated by a chopper. A filter for the visible spectrum (from 400 to 700 nm) was used to avoid the UV and NIR spectrum.

Results and discussion

The exploitation of the plasmonic effect in photovoltaic application can affect its performance by two important ways: (i) near field (strong absorption near the surface of NPs) and (ii) far field (scat- tering from NPs) enhancements, which both yield to enhance light trapping into the solar cell devices [13]. In this work, scattering of incident light from MNPs into the underlying substrate is crucial to increase the travelled optical path length of photons, leading to an enhancement in the performance of the solar cell. For this purpose, we mainly focused on self-assembled Ag-NPs with relatively large size and well-controlled distribution over the surface, which enable the high scattering phenomenon as we consider that small nanoparticles are not convenient for our study. We showed in previous work [21] that a thickness of 15 nm of silver thin film evaporated and annealed at 250°C during 1 h under argon flux gives rise to large Ag-NPs with high surface coverage rate that can ensure the scattering phenomenon. However, with the change of the under- lying layer of Ag-NPs from silicon to SnO_2, the morphology as well as the optical response of the structure can be affected. In this section, optical and morphological properties of self-assembled Ag- NPs in the presence of different thickness layer of SnO_2 (20, 50, 79, 100 and 152 nm) are discussed. Samples are fabricated at the same condition of evaporation and dewetting for optical and electrical characterization.

Figure 2 shows the total reflectance of substrates with and without Ag-NPs separated from the silicon active layers by oxide spacers with different thicknesses. The thickness of SnO_2 varies from 20 to 152 nm. We can see from samples data without Ag-NPs that peaks can be attributed to the interference between the incident and scattered lights. Clearly, the reflectance spectrum red shifts with increasing dielectric layer thickness, suggesting that the surface plasmon excitation is governed by silicon substrate when the spacer layer is sufficiently thin (20 nm). On the other hand, when the SnO_2 thickness becomes larger, the reflectance peak wavelength corresponding to the plasmon res- onance slightly changes. By increasing the thickness of SnO_2, the resonance peak of the electron clouds inside the Ag-NPs shift to higher wavelength, the reflection peak wavelength respect to the plasmon resonance increase either. The fact that when the oxide layer is thicker, the effect of silicon substrate on the surface plasmon is negligibly small, owing the essential contribution to the oxide.

It can be deduced that the reflectance in the short wavelength range is determined by the surface plasmon rather than the spacer. Reflected light is only determined by the anti-reflection film at long wavelengths, and the light scattering induced by the surface plasmon is negligible. When the oxide layer is very thin, the effect of Si on the near-field enhancement dominates owing to the localization of the surface plasmon. When the dielectric layer thickness is about 79 nm, the effect of SnO_2 is on the same order as the effect of the silicon substrate, producing two resonance peaks.

Figure 3 regroups the reflectance spectra of varied SnO_2 thickness in the presence of Ag-NPs, also one sample coated only with Ag-NPs. The presence of Ag-NPs without an anti-reflection layer indicates the presence of two resonance peaks: quadrupolar one located at 332 nm and dipolar one located at 536 nm. The use of SnO_2 as a spacer layer between Ag-NPs and silicon introduce a significant reduction in the reflectance spectra, especially for thicknesses which not exceed 100 nm.
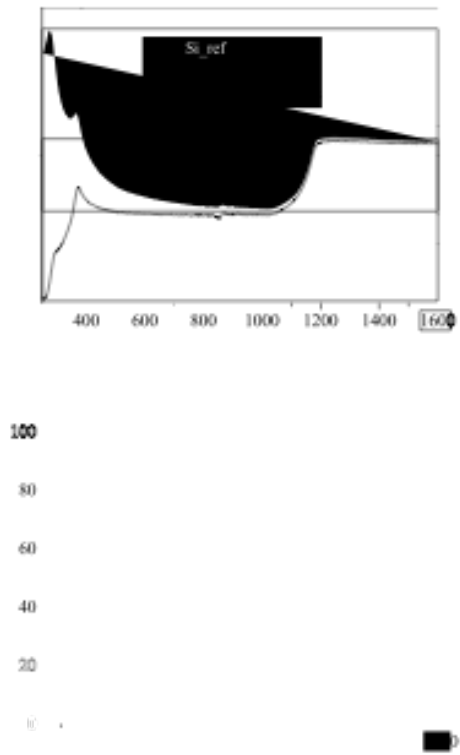
Figure 2 . Total reflectance of varied SnO₂ thickness with and without Ag-NPs.

It is well known that silicon is unable to transmit light in the UV-Vis region where surface plas- mon resonance takes place. Hence, same steps of deposition and annealing conditions are per- formed on glass substrates in order to extract information about transmitted light into the structure. For the transmittance measurements, photons that are absorbed or back-scattered by par- ticles are not detected, leading to well-defined minima in the spectra at the extinction peak wave- lengths, as extinction is the inverse of transmittance. Whilst for reflectance measurements, photons

Figure 3 . Total reflectance of varied SnO$_2$ thickness in the presence of Ag-NPs.

that are forward-scattered or absorbed by NPs will not be detected which mean that back-scattered ones will be detected in the reflectance signal.

The transmission minima (Figure 4) show the same trends as the reflectance maxima. We notice a red-shift of the reflectance in comparison with the transmittance minima. Knowing that the refractive index of glass and silicon are respectively 1.5 and 3.5, so the observed red shift is due to the increase in the refractive index of the local environment arising from proximity to the SnO_2 spacer layer.

The distribution and the size of Ag-NPs depend on their environment, i.e. the direct contact to the surface of the substrate on which they are deposited. The thickness of the deposited oxide layer (SnO_2) influences the formation of Ag-NPs and leads to varied morphologies. Figure 5 shows SEM images of Ag-NPs on varied SnO_2 thickness with their corresponding average size distribution and surface coverage rate (Sc). After the dewetting process, the continuous Ag films were congregated into small islands owing to different thermal expansion coefficients of Ag, SnO_2, and silicon. As shown in Figure 5, most of the particle sizes concentrated in the range from 20 to 200 nm, and the particles formed on the 152, 100 and 79 nm SnO_2 films had broader size distributions, while nanoparticles in other cases had a Gaussian size distribution. It can also be seen that the surface

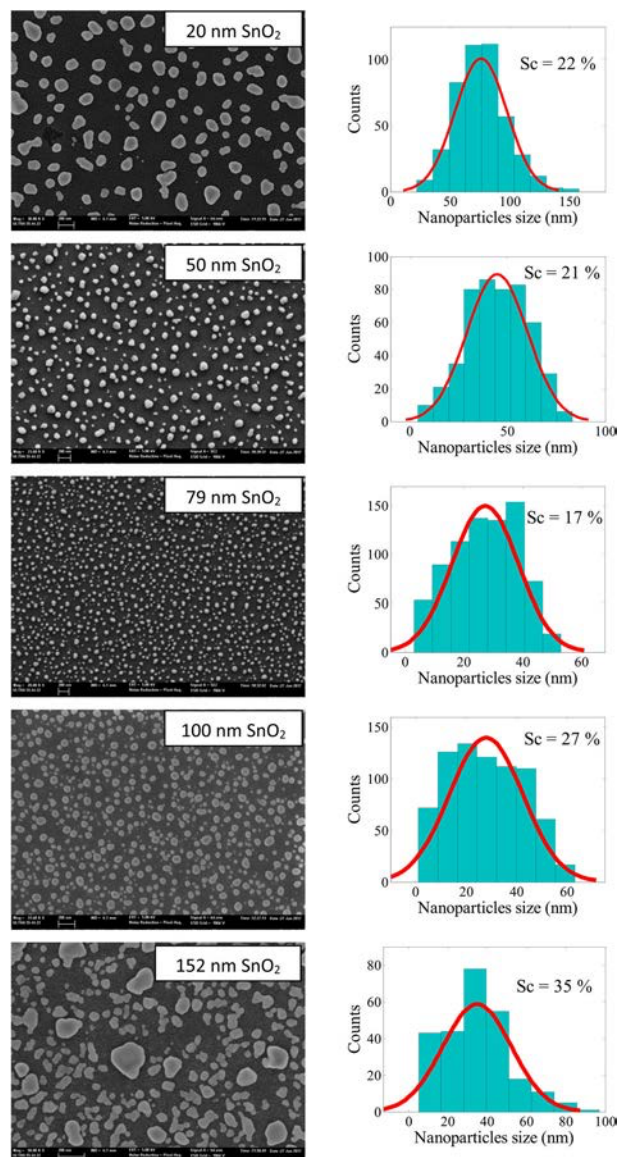Figure 4 . Transmittance spectra of varied SnO2 thickness in the presence of Ag-NPs deposited on glass substrates.

Figure 5 . SEM images of Ag-NPs on varied SnO$_2$ thickness with their average size distribution.

coverage rate of the Ag islands is maintained at 17–35%. Since the nanoparticles in the random arrays have large size distributions, the overall effect of particle diameter on the scattering behavior, when averaged over the array, is expected to be small. Thus, the factor that determines the trends observed experimentally is the presence of the oxide layer and the change in dielectric layer thick- ness. From SEM images, we can see that large Ag-NPs are formed on the sample with 20 nm SnO$_2$ thickness. Silicon has lower thermal conductivity than SnO$_2$, therefore when SnO$_2$ has 20 nm thick- nesses, the thermal conductivity of silicon governs the silver dewetting and as consequence, larger particles are formed. When we increase the thickness of SnO$_2$, the thermal conductivity of SnO$_2$ governs the dewetting of Ag-NPs and smaller NPs are formed.

Figure 6 summarize the Ag-NPs average size in function of SnO$_2$ thickness. The increase in SnO$_2$ thickness from 20 to 80 nm results in a reduction in the Ag-NPs average size. A further increase in

20   40   60   80   100   120   140   160

Figure 6 . Ag-NPs average size in function of SnO2 thickness.

this thickness from 80 to 150 nm affects essentially the distribution of Ag-NPs rather than the size. NPs deposited on a thick layer of SnO2 have a non-uniform distribution in size and shape.

The collective oscillations of electrons in metal nanoparticles excited by incident light lead to the formation of polarization charges on the particle surface, i.e. origin of the localized surface plas- mons. Plasmonic effect consists in trapping of the incident light by plasmons due either to absorp- tion and (or) scattering depending upon the nanoparticle size. The absorption by plasmons dominates for metallic particles with a size much smaller than the plasmon wavelength of light. However, as the particle size increases, plasmonic scattering prevails for light wavelength around the plasmonic resonance. The angular spread of light is accompanied by an enhancement in path length in silicon substrate and thereby increased absorption and generation of electron– hole pairs. Finally, scattering process must lead to enhanced absorption of light in the substrate and hence to a predictable conversion efficiency improvement, which will be discussed in the next section.

The electromagnetic field in our semiconductor device can be approximately interpreted as a superposition of the field arising from simple transmission across the dielectric layer (SnO_2) inter- face formed at the semiconductor (silicon) surface and that due to wavelength-dependant scattering by the Ag-NPs. The phase relationship between the field components can lead to either constructive or destructive interference within silicon and hence to either an increase or decrease in the photo- current response at different wavelengths.

To estimate the influence of Ag-NPs induced changes on the photocurrent generation in our devices, we measured the external quantum efficiency (EQE) for different samples. The EQE pre- sents the measure of the number of electrons generates per number of incident photons on the device surface, for each wavelength. Importantly, the EQE measurement is more relevant than the absorption measurement of the solar cells for determining the enhancement in the cell absorp- tion because it can decouple the light absorption in the active layer from the parasitic absorption caused by the Ag-NPs. Additionally, deposition of the Ag-NPs directly on the surface of emitter (n^+ silicon) may increase surface recombination, which would also affect the generated photocur- rent. The presence of thin dielectric spacer layer such as SnO_2 between the cell and Ag-NPs may segregate the parasitic absorption losses and interfacial charge carrier recombination by providing electronic separation. With this motivation, the Ag-NPs are prepared on cells coated with different SnO_2 thicknesses under similar conditions.

It can be seen from Figure 7, where the EQE plots are presented, that there is a clear correlation between the reflectance and the spectral response for each device. In fact, the increase in the reflec- tance results in a decrease in spectral response. In the short wavelength region, where SPR takes place, the decrease in the EQE can be attributed to the parasitic absorption losses from Ag-NPs

400   600   800   1000

Figure 7 . EQE curves for Ag-NPs with different SnO$_2$ thicknesses.

[22]. We take as a reference a cell without Ag-NPs as well as a dielectric spacer layer. For this device, the EQE is maintained broaden over the 500–800 nm region with no-pronounced peak. Now, when we compare the reference to other samples, those coated with SnO$_2$ and Ag-NPs, we observe an increase in the EQE for 52, 79 and 100 nm thickness whilst a remarkable decrease for 20 and 152 nm. The morphology of Ag-NPs and the thickness of the dielectric spacer layer play an impor- tant role in the spectral response of our devices. As presented in Figure 7, where SEM image of Ag- NPs deposited on the thin SnO$_2$ surface (20 nm of thickness), the average particle size is around 80 nm. Due its week thickness, deposited SnO$_2$ presents a non-uniform thin layer on the top surface of silicon. Discontinuous deposited SnO$_2$ film separate silicon and Ag-NPs. Hence, after the depo- sition and formation of Ag-NPs (obtained after the dewetting process), a void may be segregated between Ag-NPs and silicon substrate. This geometry can cause degradation in the performance of this cell. The same comportment is obtained for device with 152 nm SnO$_2$ thickness but this time is due to the distribution and morphology of Ag-NPs. A large thickness of SnO$_2$ yield to non-homogeneity in size and shape of Ag-NPs. SEM image of this sample shows a variety of size and shape of Ag-NPs. We can clearly observe large particles with non-spherical shape sur- rounded by small NPs. As demonstrated in the previous chapter, non-homogeneous morphology leads to an increase in the reflectance which will diminish the number of absorbed photon. Beside of the morphology and distribution of Ag-NPs, the presence of thick SnO$_2$ layer will govern the optical response, which is clearly pronounced in its reflectance spectrum.

For the other three devices, coated with Ag-NPs and 50, 79 and 100 nm of SnO$_2$, the EQE was enhanced over a broad spectral range from 700 to 950 nm with a pronounced red-shifted peak. The increase in the EQE indicates that the Ag-NPs can strongly enhance absorption in the photoactive layer and hence lead to an increase in the photocurrent. The slight decrease in the EQE outside the wavelength range of 700–950 nm can be attributed to the back-scattering effect.

The improvement in spectral response is further illustrated by different electrical parameters of our full devices scale, calculated from J(V) curves. These parameters are summarized in Table 1. As we obtain the best enhancement in EQE for cell coated with 100 nm SnO_2 and Ag-NPs, we will limit our interest to compare its electrical parameters to other cells with and without Ag-NPs, in order to evaluate the plasmonic effect on the efficiency. Figure 8 shows the current density–voltage corre- sponding power output curves of cells: with SnO_2 and Ag-NPs, with only Ag-NPs and a reference cell without oxide and Ag-NPs. To obtain the enhancement of different structures, the efficiency of solar is calculated and then compared to the efficiency of the reference solar cell. Small changes in the V_{oc} were observed (from 0.5 to 0.53 V) in the measurements from sample to sample, most likely

Table 1. Electrical characteristics of fabricated silicon solar cells.

Cell	V_{oc} (V)	J_{sc} (mA/cm^2)	FF (%)	V_{max} (V)	I_{max} (mA)	R_{sh} (Ω)	R_s (Ω)	η (%)
Ref	0.5	19.12	49	0.32	36.09	257.9	3.41	4.81
Ag-NPs	0.51	21.57	45	0.32	39.54	48.78	3.88	5.06
SnO_2/Ag-NPs	0.53	27.61	39	0.32	45	20.02	3.6	6.14

0.02

0.00

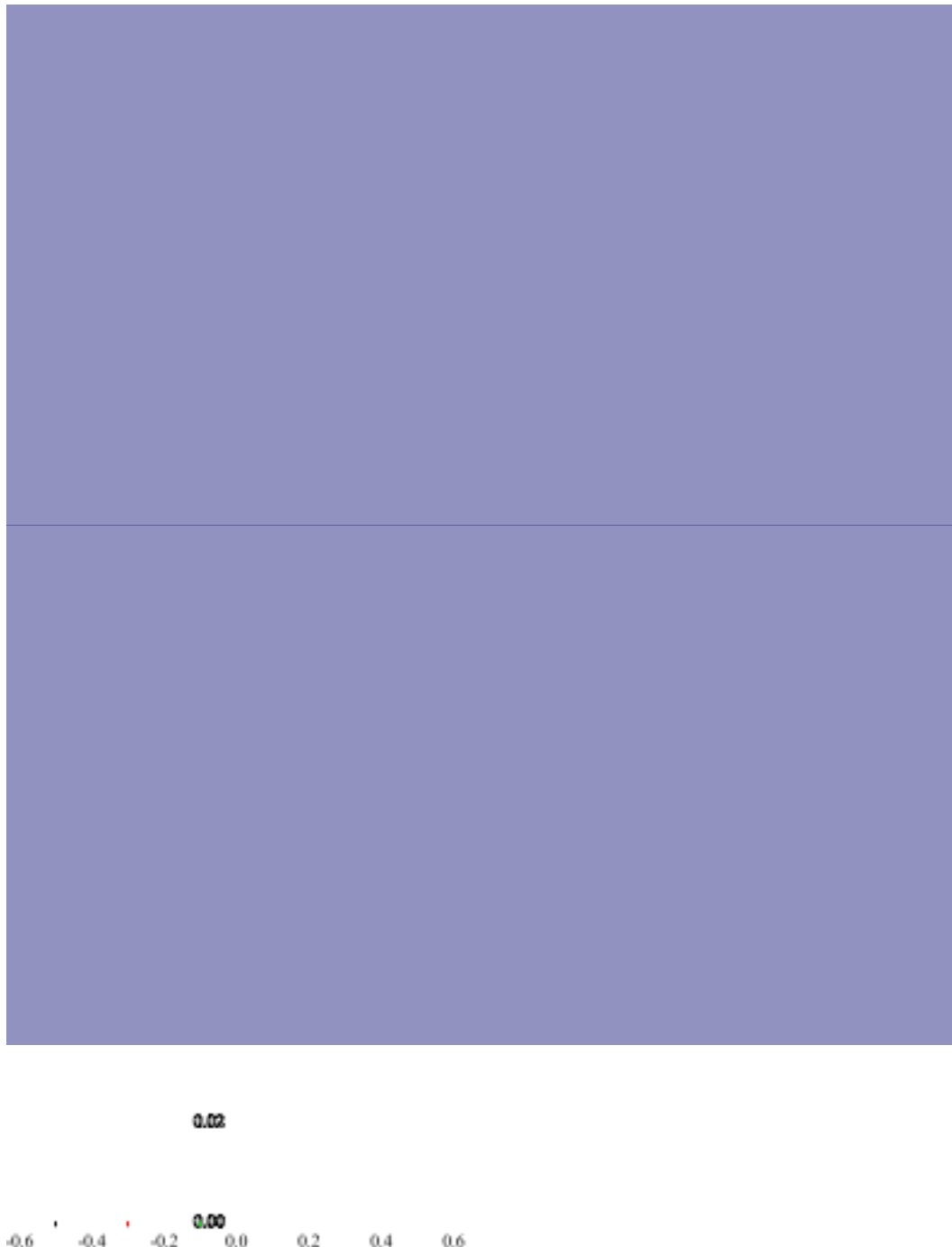-0.6   -0.4   -0.2   0.0   0.2   0.4   0.6

Figure 8 . Current density–voltage characteristic of fabricated cells. The thickness of SnO_2 spacer layer is 100 nm.

due to non-ideal of fabrication and nature of p-n junction (partial redistribution of uncontrolled

impurities from p-n junction region). Overall, the observed minimal variations in V_{oc} suggest

that the placement of Ag-NPs coated with SnO_2 on the photovoltaic device surface influences pre-

dominantly I_{sc} and that η is directly proportional to ΔJ_{sc}. The current density–voltage characteristic

curves of solar cells coated with Ag-NPs unambiguously confirm the effectiveness of plasmonic

scattering in improving J_{sc} and η of the device. As expected, the largest enhancement was achieved 2

by Ag-NPs coated with 100 nm of SnO_2 with a relative increase in J_{sc} from 19.12 to 27.61 mA/cm . This improvement is consistent with the reflectance reduction and EQE enhancement presented previously in Figures 3 and 7, respectively. We observe for device incorporating Ag-NPs that R_{serie} is mush high comparing to reference and device coated with SnO_2 confirming that deposition of Ag-NPs directly on the surface of emitter (silicon n$^+$) may increase recombination as the metal is in direct contact with silicon. The energy conversion efficiency is increased clearly from 4.81% to 6.14% corresponding to a 1.33% enhancement compared to the same cell coated with both SnO_2 and Ag-NPs. So, plasmonic Ag-NPs in the presence of 100 nm of SnO_2 have effect on mini- mizing reflection and increasing light trapping by helping light to stay longer in the active area of the cell, these properties can lead to higher efficiencies through increasing absorption and generat- ing more current in the solar cell devices.

Conclusions

In this work, we have studied the integration of Ag-NPs in the presence of dielectric spacer layer (SnO_2) in silicon-based solar cells and investigated their optical and electrical properties. The use of Ag-NPs in the presence of a dielectric spacer layer can play an important role in minimizing reflection and increasing light trapping by helping light to stay longer in active solar cell layers.

Light trapping is key a factor for improving the current and cell efficiency. It has been demonstrated that randomly distributed Ag-NPs deposited on top surface of 100 nm of SnO_2 leads to obvious broadband light trapping over spectral wavelength from 600 to 950 nm. Significant photocurrent and conversion efficiency enhancement was observed due to the plasmonic enhanced scattering. Front located nanoparticles on thick spacer layers (not beyond 100 nm for SnO_2) represent a prom- ising light-trapping approach for the enhancement of the current and the increase of the cell efficiency.

Acknowledgment

Disclosure statement

No potential conflict of interest was reported by the author(s). Funding

References

1. [1] Gielen D, Boshell F, Saygin D, et al. The role of renewable energy in the global energy transformation. Energy Strategy Rev. 2019;24:38–50.
2. [2] Yang D, Yang R, Wang K, et al. High efficiency planar-type perovskite solar cells with negligible hysteresis using EDTA-complexed SnO2. Nat Commun. 2018;9:3239.
3. [3] Cui Y, Yao H, Zhang J, et al. Over 16% efficiency organic photovoltaic cells enabled by a chlorinated acceptor with increased open-circuit voltages. Nat Commun. 2019;10:2515.
4. [4] Li X, Pan F, Sun C, et al. Simplified synthetic routes for low cost and high photovoltaic performance n-type organic semiconductor acceptors. Nat Commun. 2019;10:519.

5. [5] Bhattacharya S, John S. Beyond 30% conversion efficiency in silicon solar cells: a numerical demonstration. Sci Rep. 2019;9:12482.
6. [6] Wang D, Su G. New strategy to promote conversion efficiency using high-index nanostructures in thin-film solar cells. Sci Rep. 2014;4:7165.
7. [7] Catchpole KR, Polman A. Plasmonic solar cells. Opt Express. 2008;16:21793–21800.
8. [8] Liu W, Wang X, Li Y, et al. Surface plasmon enhanced GaAs thin film solar cells. Sol Energy Mater Sol Cells.

   2011;95:693–698.

9. [9] Shah AV, Vaněček M, Meier J, et al. Basic efficiency limits, recent experimental results and novel light-trapping

   schemes in a-Si:H, µc-Si:H and `micromorph tandem' solar cells. J Non-Cryst Solids. 2004: 338–340.:639–645.

10. [10] Shah AV, Schade H, Vanecek M, et al. Thin-film silicon solar cell technology. Prog Photovolt Res Appl.

   2004;12:113–142.

11. [11] Schaadt DM, Feng B, Yu ET. Enhanced semiconductor optical absorption via surface plasmon excitation in

   metal nanoparticles. Appl Phys Lett. 2005;86:063106.

12. [12] Pillai S, Catchpole KR, Trupke T, et al. Surface plasmon enhanced silicon solar cells. J Appl Phys.

   2007;101:093105.

13. [13] Atwater HA, Polman A. Plasmonics for improved photovoltaic devices. Nat Mater. 2010;9:205–213.
14. [14] Adamovic N, Schmid U. Potential of plasmonics in photovoltaic solar cells. E Elektrotechnik

Informationstechnik. 2011;128:342–347.

15. [15] Zhong S, Zeng Y, Huang Z, et al. Superior broadband antireflection from buried Mie resonator arrays for high- efficiency photovoltaics. Sci Rep. 2015;5:8915.
16. [16] Kelly KL, Coronado E, Zhao LL, et al. The optical properties of metal nanoparticles: the influence of size, shape, and dielectric environment. J Phys Chem B. 2003;107:668–677.
17. [17] Pillai S, Beck FJ, Catchpole KR, et al. The effect of dielectric spacer thickness on surface plasmon enhanced solar cells for front and rear side depositions. J Appl Phys. 2011;109:073105.
18. [18] Xu R, Wang X, Liu W, et al. Optimization of the dielectric layer thickness for surface-plasmon-induced light absorption for silicon solar cells. Jpn J Appl Phys. 2012;51:042301.
19. [19] Xu R, Wang X-D, Liu W, et al. Dielectric layer-dependent surface plasmon effect of metallic nanoparticles on silicon substrate. Chin Phys B. 2012;21:025202.
20. [20] Schneider CA, Rasband WS, Eliceiri KW. NIH image to ImageJ: 25 years of image analysis. Nat Methods. 2012;9:671–675.
21. [21] Manai L, Rezgui BD, Bou A, et al. Enhanced light trapping using plasmonic nanoparticles. J Phys Conf Ser. 2015;596:012002.
22. [22] Tran HN, Nguyen VH, Nguyen BH, et al. Light trapping and plasmonic enhancement in silicon, dye-sensitized and titania solar cells. Adv Nat Sci Nanosci Nanotechnol. 2016;7:013001.